Impact of the inherent structural characteristics of AA2024-T3 and D16 AM aircraft alloys on the cerium oxide primer layers morphology

Stephan Kozhukharov, Mariano Jose Milanes, Christian Girginov

Abstract: *The corrosion protection of fuselages via deposition of multilayered coating systems is an indispensable practice in the aircraft industry. Each conventional coating system in the aircraft and automobile industry is composed by multitude of layers, and every layer possesses its own specific function. In this sense, the primer layers serve for improvement of the adhesion between the metallic substrate and the upper and finishing coatings. On the other hand, when an electrochemical method is applied for primer layer deposition, the substrate alloy structure and composition have a great impact over the primer layer deposition process, and the respective primer layer features and performance. The present brief study is devoted on the comparison of the morphological features of cerium oxide primer layers electrodeposited on two different alloys with identical compositions.*

Key words: Cerium oxide primer layers, AA2024-T3, D16 AM, galvanostatic deposition.

INTRODUCTION

Recently, besides in the aircraft industry [1-3], the aluminium alloys have found continuously increasing applications for car body panels [4], and even in the modern ship-building [5, 6]. Besides, it is a common practice to apply multilayered coating systems for corrosion protection of metallic details, assemblies, and entire vehicle constrictions [7, 8].

The nowadays advanced coating systems should owe capabilities for active corrosion protection, in addition to the necessary barrier ability and durability [9, 10]. Indeed, the advanced coatings should possess additional properties, in order to remain its protective properties even after coating damage. Thus, in the literature can be found investigations on: self-healing ability [8], capability for gradual corrosion inhibitor release in the already damaged areas [9 – 11], hydrophobicity [12], sunlight induced ageing resistance [13], etc.

In this sense, the aim of the present study is to observe the impact of the substrate structural features on the morphology of the obtained cerium oxide primer layers (CeOPL).

EXPERIMENTAL

Deposition procedure – Since the coating deposition procedure is identical to the used in previous works [14, 15], it will be described only in brief, here. Thus, all the coatings were deposited in galvanostatic regime maintained by PG/stat 30-2 “Autolab” product of Ecochemie (the Netherlands), with cathodic current density: I = -2 mA/cm^2 for 240 seconds. The depositions were performed in three electrode flat cell, with silver chloride referent electrode, and SS 316 horseshoe counter electrode. The depositions were performed by coincident potential recording. The exposed area of the metallic substrates (i.e. the working electrode) was 11.95 cm^2. The deposition electrolyte was 100 ml. 0.03 M diammonium pentanitrocerate solution with 0.7 ml addition of 30% H_2O_2 as deposition activator. All the metallic substrates have undergone preliminary treatment, at the same conditions, as described in a previous work [16]. In brief, alkaline etching in 50g/l NaOH at 50 ºC for 2 minutes and subsequent acidic activation in HNO_3 (1:1) at room temperature for 10 minutes were applied.

Sample observations – Systematic sample observations were executed, in order to determine the correlation between the structural features of the used metallic substrates and these of the cerium oxide deposits. Thus, the specimens were observed by optical microscopy, with image magnification x 40, by optical microscope Boeco (Germany), The SEM images were obtained using a scanning electron microscope TESCAN, SEM/FIB LYRA I XMU. The local composition was studied using energy dispersion X-ray spectroscopy, EDX (Quantax 200 of BRUKER detector) connected to the SEM-device.

RESULTS AND DISCUSSION

In-situ chronopotentiometric curves

During the coating depositions, chronopotentiometric curves were recorded, against Ag/AgCl reference electrode. As can be seen in Fig. 1, in both cases the curves possess relatively similar shapes, but the current density, necessary for coating deposition (i.e. -2 mA/cm^2) is reached at different potential intervals.

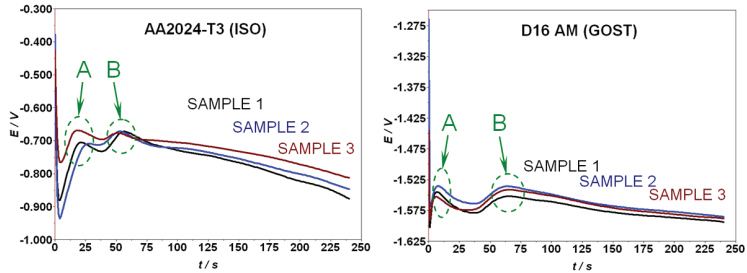

Fig. 1. In-situ chronopotentiometric curves recorded during the coating deposition versus Ag/AgCl referent electrode

The similarity between the shapes of the curves, recorded during the coating depositions is due to the similar compositions of the alloy substrates, [17, 18], but the difference between the respective potentials is obvious consequence of the structural features of each alloy. Indeed, according to GOST 4784-97, the D 16 AM alloy is additively tempered, annealed and artificially aged, so that a thicker oxide layer is formed on its surface. This oxide layer has a greater electrical resistance which should be overcome, in order to achieve the necessary current density. This fact has stimulated the more detailed observations, described below.

Surface observations

Because of the different thermal cycling, the corresponding alloys possess different granulometric compositions, which predetermine distinguishable behaviour of their surfaces in contact with aggressive solutions (e.g. the NaOH solution during the etching). Indeed, in the literature, it is pointed, that the larger grain size predetermines deeper penetration of the intergrannular corrosion through the grain boundaries, whereas the smaller grains predetermine more even subsurface intergrannular corrosion impact distribution. Besides, during this preliminary treatment process, intermetallic component dissolution and re-deposition proceed, followed by removal of the obtained metal oxide black smut, during the subsequent desmutting with HNO_3. All these processes during the preliminary alloy treatment predetermine the surface roughness, and compositional distribution of the respective alloys. The optical micrographs (Fig. 2) reveal that the tempered alloy D16 AM possesses relatively smoother surface, compared to AA2024-T3.

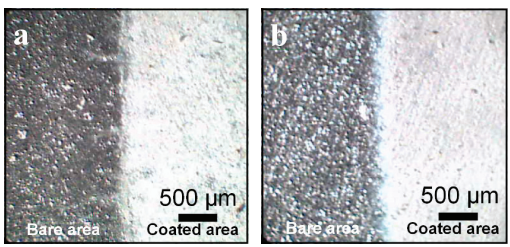

Fig. 2. Optical micrographs of D16 AM and AA2024-T3

This fact is confirmed by the SEM/EDX images in Figs. 3 and 4. Besides, the images reveal that irrespective the smoother bare surface of D16 AM, its coating looks agglomerated and less uniform, compared to this of AA2024-T3. The possible reason for this fact might be the thicker oxide layer, formed during the thermal post-treatment, which is randomly disrupted on the areas in vicinity to the superficial intermetallic inclusions. Another possible reason could be that the larger sized grains of the basic Al-matrix predetermine larger distances among these intermetallics, which in this case serve as coating nucleation initiators. Regardless the several coarse particles, observable on the coated area of AA2024-T3 (Fig. 3b), its coating is in form of thin regular film, due to both the thinner oxide layer and the shorter distances among the intermetallics, as a result of the finer granulometric structure of the basic aluminium matrix, predetermined by the sharp solidification of this alloy during its rolling.

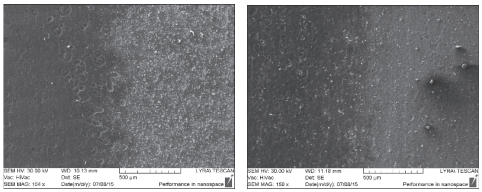

Fig. 3. SEM images of D16 AM and AA2024-T3

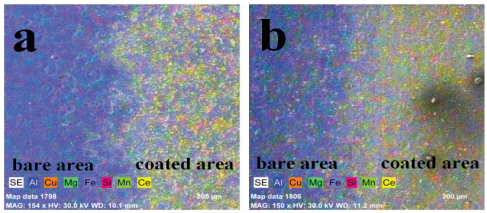

Fig. 4. EDX maps of D16 AM and AA2024-T3

Another interesting feature is the occurrence of caverns on the D16 AM surface, as a result of crevice and/or exfoliation corrosion phenomena, during the preliminary treatment. It also could be explained by the larger size of the grains of the basic aluminium matrix. However, both alloys possess corrosion pits, which according to the literature [19, 20] are the most typical localised corrosion form for this class of materials. Especially, in the Cu-Mg containing alloys such as AA2024 and D16 types, the pitting corrosion appears as a result of presence of elements, nobler than the aluminium matrix. Thus, the aluminium dissolution proceeds preferentially adjacent to the intermetallic precipitates, and especially inside and around the the S-phase (Al_2CuMg) and θ-phase (Al_2Cu) inclusions. Afterwards, it propagates on the less active cathodic zones, such as $Al_{20}Cu_2(Fe\ Mn)_3$ [21 - 23]. These particles serve as cathodic areas, which cause further enhancement of the alkalinity in their surrounds, during the preliminary treatment procedures. This effect is a result of the cathodic reduction of the oxygen, dissolved in the liquid medium, which leads to OH^- generation. In contrary, according to the well illustrated model, proposed by Lau et al. [24], during the CeOPL deposition, namely these cathodic areas serve as nucleation of cerium oxide deposition. This model is also denominated as “island like growth mechanism” by Arnott and co. [25]. Having in mind this concept, it can be assumed that the copper rich S-phase and θ-phase inclusions, followed by the less active cathodic domains described above serve for CeOPL deposition initiation centres (positions “A” and “B” in Figure 1, respectively).

CONCLUSIONS

Besides, at galvanostatic regime, the required current density in the case of AA2024-T3 is achieved at lower (as modulus) potentials than for D16 – AM. This fact is an indication for the thicker oxide layer possessed by the latter alloy. This layer is formed during the metallurgical post-treatment procedures. It reveals a higher electrical resistance, imposing by that manner a higher (as modulus) potential applied for reaching of the required current density.

Nevertheless, in both cases, the curves possess identical shapes, because of the identical chemical compositions of the respective alloys.

The almost complete overlapping among the deposition curves acquired during the depositions on D16-AM, revealing high repeatability rate is a result of the more uniform distribution of the intermetallic particles, due to the annealing of this alloy in the process of its metallurgical production.

The sharp cooling of AA2024-T3, via cold rolling results in sharp solidification, and predetermines smaller grain size, and more uniform distribution of the intermetallics. These structural features predetermine more even distribution of the coating layer, which grows as continuous cerium oxide film. In contrary, the CeOPL, deposited on the surface of D16 AM, is strongly aggregated, due to the larger distances among the intermetallics predetermined by the larger grain size of the Al-matrix grains, formed during the thermal post-treatment procedures. Besides, the oxide layer of this alloy is also thicker and denser, due to these additional metallurgical operations, and disturbs the CeOPL deposition. The next electrochemical investigations will show whether this thicker oxide layer contributes to the overall corrosion protection of the CeOPL coated D16 AM alloy.

Acknowledgements: The present research work has been performed by the financial support of the Bulgarian National Scientific Fund, Project T 02 – 27. This study is devoted in memoriam of Dr. Dimitar Chalev.

REFERENCES

[1] Wildey, J. F., Aging Aircraft, Materials Performance, 1990, 29, 80–85

[2] Komorowski, J. P., et al., Quantification of Corrosion in Aircraft Structures with Double Pass Retroreflection, Canadian Aeronautics and Space Journal, 1996, 42, 76–82

[3] Starke E. A., Jr., and J. T. Staley, Application of Modern Aluminum Alloys to Aircraft, Prog. Aerospace Sci., 1996, 32, 131-172

[4] Davies G., Materials for Automobile Bodies, Linacre House, ed. (2003), ISBN 0 7506 5692 1, pp. 146 – 156.

[5] Eyres D., “Ship construction”, 6th ed. 2007, Linacre House, p. 50–52, ISBN 10:0-75-068070-913.

[6] “Aluminium in shipbuilding”, access via: http://www.aluminiumleader.com/en/around/transport/ship

[7] Balgude D., A. Sabnis, Sol–gel derived hybrid coatings as an environment friendly surface treatment for corrosion protection of metals and their alloys, J. Sol-Gel Sci. Technol. DOI 10.1007/s10971-012-2838-z

[8] Stankiewicz A., I. Szczygiel, B. Szczygiel, Self-healing coatings in anti-corrosion applications, J. Mater. Sci. 2013, 48, 8041–8051

[9] Kozhukharov S., V. Kozhukharov, M. Wittmar, M. Schem, M. Aslan, H.Caparrotti, M.Veith, Protective abilities of nanocomposite pre-treatments containing Al_2O_3 nano-particles loaded by $CeCl_3$, Prog. Org. Coat., 2011, 71, (2), 198-205

[10] Kozhukharov S., V. Kozhukharov, M. Schem M. Wittmar, M. Veith, Protective ability of hybrid nano-composite coatings with cerium sulphate as inhibitor against corrosion of AA2024 aluminium alloy, Prog. Org. Coat. 2012, 73, (1), 95-103

[11] Matter E., S. Kozhukharov, Correlation between preliminary pretreatments and the behaviour of AA2024 – aluminium alloy in 3.5% NaCl model corrosive medium, Annual proceedings of "Angel Kanchev" University of Ruse (Bulgaria), 2010, 49, 14 – 19. access via: http://conf.uni-ruse.bg/bg/docs/cp10/9.1/9.1-2.pdf

[12] Arellanes-Lozada P., O. Olivares-Xometl, D. Guzmán-Lucero, N. V. Likhanova, M. A. Domínguez-Aguilar, I. V. Lijanova, E. Arce-Estrada, The Inhibition of Aluminum Corrosion in Sulfuric Acid by Poly(1-vinyl-3-alkyl-imidazolium Hexafluorophosphate), Materials, 2014, 7(8), 5711-5734

[13] Bubev E., V. Bozhilov, S. Kozhukharov, M. Machkova, V. Kozhukharov, Flexible UV-absorbing films-deposition and charaterization, Journal of International Scientific Publications: Materials, Methods and Technologies, V. 8, ISSN 1314-7269.

[14] Kozhukharov S., J.A.P. Ayuso, D.S. Rodríguez, O.F. Acuña, M. Machkova, V. Kozhukharov, Optimization of the basic parameters of cathodic deposition of Ce-conversion coatings on D16 AM clad alloy, J. Chem. Technol. Metall., 2013, 48, 3, 296-307

[15] Ayuso J. A., S. Kozhukharov, M. Machkova, V. Kozhukharov, Electrodeposition of cerium conversion coatings for corrosion protection of D16 AM clad alloy, Bul. Chem. Commun. 2013, 45, (Spec. Issue-A), 33-40

[16] Gil T.P., S. Kozhukharov, C. Girginov, Deposition of cerium conversion coatings on AA2024-T3 aircraft alloy at fixed potentials, Annual Proceedings of "Angel Kanchev"University of Ruse (Bulgaria), 2014, 53, 9–13, access via: http://conf.uni-ruse.bg/bg/docs/cp14/10.1/10.1-1.pdf

[17] Internet access via: "Avek Global": http://www.avglob.biz/grade-list/257-m-D16.html

[18] Internet access via: "ASM Aerospace Specification Metals, Inc": http://asm.matweb.com/search/SpecificMaterial.asp?bassnum=MA2024T4

[19] Blanc C., B. Lavelle, G. Mankowski, The role of precipitates enriched with copper on the susceptibility to pitting corrosion of the 2024 aluminium alloy, Corros. Sci. 1997, 39, (3), 495–510

[20] Guillaumin V., G. Mankowski, Localized corrosion of 2024 T351 aluminium alloy in chloride media, Corros. Sci. 1998, 41, (3), 421–438

[21]] Boag A., A.E. Hughes, A.M. Glenn, T.H. Muster, D. McCulloch, Corrosion of AA2024-T3 Part I: Localised corrosion of isolated IM particles, Corros. Sci., 2011, 53, 17-26

[22] Hughes A.E., A. Boag, A.M. Glenn, D. McCulloch, T.H. Muster, C. Ryan, C. Luo, X. Zhou, G.E. Thompson, Corrosion of AA2024-T3 Part II: Co-operative corrosion, Corros. Sci. 2011, 3, 27-39

[23] Antony T. R., Determining the probability of stable pit initiation on aluminium alloys using potentiostatic electrochemical measurements, Corros. Sci., 2005, 47, 2240-2256

[24]. Lau D., A.M. Glenn, A.E. Hughes, F.H. Scholes, T.H. Muster, S.G. Hardin, Factors influencing the deposition of Ce-based conversion coatings, Part II: The role of localised reactions, Surf. Coat. Technol., 2009, 203, 2937–2945

[25] Arnott D. R., N. E. Ryan, B. R. W. Hinton, B. A. Sexton, A. E. Hughes, Auger and XPS studies of cerium corrosion inhibition on 7075 aluminum alloy, Appl. Surf. Sci. 1985, 22/23, 236-251. DOI: 10.1016/0378-5963(85)90056-X

About the author:

Dipl. Eng. Stephan Kozhukharov Ph. D. University of Chemical Technology and Metallurgy (Sofia), E-mail: stephko1980@abv.bg.

This paper has been reviewed